Brazilian Journal of Analytical Chemistry
Pre-publication – Accepted after peer review
doi: 10.30744/brjac.2179-3425.AR-114-2025

BrJAC

ARTICLE

Laser-Induced Graphene Electrodes for the Voltammetric Determination of Ciprofloxacin in Pharmaceutical and Water Samples

Daniela Nunes da Silva[1], Ângelo Rafael Machado[2], Thaís Cristina de Oliveira Cândido[1], Lucas Franco Ferreira[2], Arnaldo César Pereira[1]*

[1]Universidade Federal de São João del-Rei (UFSJ), Departamento de Ciências Naturais. Praça Dom Helvécio, 74. São João del Rei, MG, 36301-160, Brazil

[2]Universidade Federal dos Vales do Jequitinhonha e Mucuri (UFVJM), Campus JK, Diamantina, MG, 39100-000, Brazil

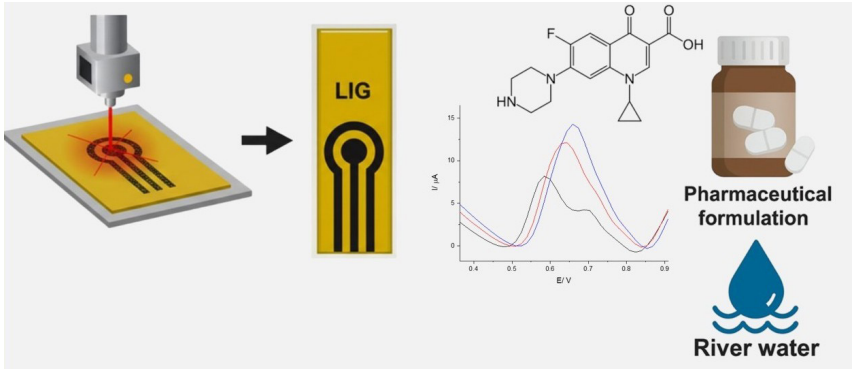

This study reports a laser-induced graphene (LIG) electrode as a simple platform for the determination of ciprofloxacin (CPX). LIG was fabricated by laser scribing a Kapton® polyimide tape affixed to a ceramic substrate. Under optimized conditions, phosphate buffer as supporting electrolyte (0.10 mol L^{-1}, pH 7.0), and differential pulse voltammetry (pulse amplitude 60 mV, scan rate 30 mV s^{-1}), the method delivered a linear response from 8.3 to 166.7 µmol L^{-1}, with limits of detection and quantification of 2.5 and 8.3 µmol L^{-1}, respectively. The procedure was successfully applied to a pharmaceutical formulation and river water, yielding recoveries of 92.93–110% with good precision, thereby demonstrating the robustness of the method. The proposed LIG sensor is a cost-effective and sustainable alternative for environmental and quality control monitoring of CPX.

Keywords: laser-induced graphene, electrochemical sensor, ciprofloxacin, pharmaceutical analysis, environmental water

INTRODUCTION

Ciprofloxacin (CPX) is a fluoroquinolone antibiotic widely prescribed for treating bacterial infections in humans and animals. Its extensive use has raised significant environmental and health concerns, as up to 70% of the administered dose can be excreted unchanged.[1,2] This persistence contributes to the development of antibiotic resistance and increases the risk of environmental contamination. CPX residues

Cite: da Silva, D. N.; Machado, A. R.; Cândido, T. C. O.; Ferreira, L. F.; Pereira, A. C. Laser-Induced Graphene Electrodes for the Voltammetric Determination of Ciprofloxacin in Pharmaceutical and Water Samples. *Braz. J. Anal. Chem.* (Forthcoming). https://doi.org/10.30744/brjac.2179-3425.AR-114-2025

Received: November 26, 2025; **Revised:** February 20, 2026; February 25, 2026; **Accepted:** March 2, 2026; **Published online:** April 2026.

This article was submitted to the BrJAC Special Issue dedicated to Prof. Dr. Lauro Tatsuo Kubota.

have been detected in domestic sewage, hospital effluents, and animal-derived products such as milk and meat, underscoring the urgent need for simple, sensitive, and reliable analytical methodologies to monitor this compound in diverse matrices.[3-5]

CPX has been quantified using various analytical methods, including spectrofluorometry, chromatographic separation, and capillary electrophoresis.[6-12] Although these approaches offer high sensitivity and selectivity, they typically require expensive instrumentation and time-consuming sample preparations. Conversely, electroanalytical techniques, particularly voltammetry and amperometry, have gained prominence owing to their operational simplicity, low cost, and the favorable redox behavior of CPX.[13-15] Accordingly, electrochemical sensors have emerged as promising alternative for CPX quantification.

In this context, the sensor performance depends on the electrode material and the electrode–electrolyte interface. Graphene-based nanomaterials have been widely investigated for the development of electrochemical sensors because of their large surface area, high conductivity, and excellent charge transfer properties. However, there are limitations, such as complex and costly synthesis routes in conventional fabrication techniques, such as photolithography and chemical vapor deposition (CVD), as discussed by Nasraoui et al., together with the challenge of integrating the material into the device without impairing conductivity, which is directly linked to the sensitivity.[16]

In response to these limitations, laser-induced graphene (LIG) has emerged as a low-cost, fast-processing alternative.[17-20] Specifically, in electrochemical platforms, LIG combines flexibility and versatility (also relevant in wearable electronics and biosensors)[21] with high conductivity arising from sp^2 domains, lower ohmic resistance, and low charge transfer resistance, which favor accelerated electron-transfer kinetics.[16,22,23]

In this study, we report the application of an LIG-based electrochemical sensor for the voltammetric determination of ciprofloxacin. The proposed approach provides a simple, disposable, and analytical platform for quantifying CPX in pharmaceutical formulations and river water.

MATERIALS AND METHODS

Reagents

Dibasic sodium phosphate heptahydrate, monobasic sodium phosphate monohydrate, acetic acid, boric acid, and hydroquinone were obtained from Synth (Diadema, SP, Brazil). Phosphoric acid was purchased from Qhemis (Indaiatuba, SP, Brazil). Trizma® and ciprofloxacin were obtained from Sigma-Aldrich (St. Louis, MO, USA). Anhydrous magnesium sulfate was supplied by Vetec Química Fina (Duque de Caxias, RJ, Brazil). Commercial pharmaceutical tablets containing tetracycline hydrochloride (500 mg) and amoxicillin (500 mg) were obtained from Prati-Donaduzzi (Toledo, PR, Brazil). Ciprofloxacin hydrochloride (500 mg) was obtained from Laboratório Globo (São José da Lapa, MG, Brazil). Potassium ferricyanide ($K_3[Fe(CN)_6]$) and potassium ferrocyanide ($K_4[Fe(CN)_6]$) were obtained from Neon (Suzano, SP, Brazil). Potassium chloride (KCl) was purchased from Êxodo Científica (Sumaré, SP, Brazil) and used as it was received.

All reagents were of analytical grade, and solutions were prepared using ultrapure water (18.2 MΩ·cm) from a Milli-Q system (Millipore Inc., USA).

Fabrication of LIG electrodes

The electrodes were fabricated by direct laser irradiation on polyimide (Kapton®) films fixed on a ceramic substrate, as previously reported by Machado et al. (2024).[24] Raman and SEM characterization of the LIG produced under these conditions was reported in the same study, confirming its graphenic structure and porous morphology. The surface was irradiated with a KKcare A5M50 laser engraver (5.5 W maximum output) under the following optimized conditions: 29.2% maximum laser power, laser scan rate of 2729.8 mm min^{-1}, focal distance of 7.59 mm, and line density of 16.7 lines mm^{-1}. This procedure yielded a three-electrode electrochemical system comprising a reference, working, and counter electrode. To prepare the pseudo-reference electrode, Ag/AgCl ink was applied to the surface of one of the conductive traces, and an insulating layer was applied to delimit the area of the working electrode.

Under these fabrication conditions, the estimated material cost per sensor was approximately USD 0.015 per unit, based on the consumption of 35 mm of polyimide tape, 0.8 mg of Ag/AgCl, and 6 mg of insulating material per device.

The activation of the LIG electrode surface was carried out by chronoamperometry in a 0.5 mol L^{-1} phosphate buffer solution (pH 7.2) at a potential of −1.1 V for 60 s.

Electrochemical measurements

Electrochemical measurements were performed using a Multi-Potentiostat/Galvanostat PGSTAT101 equipped with an FRA32M impedance module (Metrohm Autolab B.V., Utrecht, The Netherlands). Potential control and data acquisition were performed using the Nova 2.1 software (Metrohm Autolab B.V., Utrecht, The Netherlands). All experiments were conducted in a conventional electrochemical cell containing 12.0 mL of supporting electrolyte using the LIG-based device, which integrated the working, counter, and pseudo-reference electrodes (Figure 1).

Figure 1. Image of the LIG-based device fabricated on a polyimide tape, comprising (1) a working electrode, (2) a pseudo-reference electrode, and (3) a counter electrode.

Electrochemical impedance characterization

Electrochemical impedance spectroscopy (EIS) was performed using a 5 mmol L^{-1} ferri/ferrocyanide redox probe ($[Fe(CN)_6]^{3-/4-}$, 1:1) prepared in 0.1 mol L^{-1} KCl. Spectra were recorded at the open-circuit potential after 60 s of stabilization, initiating the acquisition when $|dE/dt| \leq 1 \times 10^{-6}$ V s^{-1}. A 10 mV AC perturbation was applied from 50 kHz to 0.05 Hz with 61 logarithmically spaced frequencies (approximately 10 points/decade).

Optimization of experimental parameters for CPX detection

To optimize the electrochemical detection of CPX, cyclic voltammetry (CV) was used to identify the appropriate working potential. Measurements were performed within a potential range of −0.4 to 1.2 V at a scan rate of 50 mV s^{-1}. Subsequently, the influence of the experimental parameters on CPX detection was investigated systematically. The effect of pH was examined in Britton–Robinson buffer (0.1 mol L^{-1}) over the range of 4.0–10.0. The composition of the supporting electrolyte was evaluated by comparing Britton–Robinson, phosphate, and Trizma buffers. In addition, the ionic strength was assessed by varying the supporting electrolyte concentration from 0.05 to 0.3 mol L^{-1}.

Following these preliminary studies, differential pulse voltammetry (DPV) was used to construct an analytical calibration curve for the CPX. The optimization of the DPV parameters focused on the pulse amplitude (30–70 mV) and scan rate (10–40 mV s^{-1}). The optimal conditions (pulse amplitude of 60 mV and scan rate of 30 mV s^{-1}) were selected based on the voltammetric profile and maximum anodic peak current intensity in the presence of CPX. These optimized parameters were subsequently applied to analytical determinations.

Obtaining the analytical curve

After optimizing the experimental and operational parameters, an analytical curve was obtained by successively adding a standard CPX stock solution (20 mmol L^{-1}). From this calibration curve, the main analytical figures of merit were determined, including the linear response range, limit of detection (LOD), and limit of quantification (LOQ).

Assessment of selectivity

The selectivity of the proposed LIG sensor for CPX determination was evaluated by investigating its response in the presence of potentially interfering species commonly found in pharmaceutical formulations and environmental samples. Magnesium ions (Mg^{2+}), a typical excipient in drug formulations, were selected as representative inorganic interferents. Other widely used antibiotics, including tetracycline hydrochloride and amoxicillin, were considered because of their frequent occurrence in environmental water. Hydroquinone and diclofenac were selected as representative organic contaminants frequently detected in aquatic environments. For all experiments, the CPX concentration was fixed at 25.0 µmol L^{-1}, and each potential interferent was added at a 100-fold higher concentration. This excess was deliberately adopted to provide a stringent, worst-case evaluation of selectivity. In environmental matrices, coexisting antibiotics and organic contaminants are typically present at concentrations comparable to or lower than CPX, whereas pharmaceutical excipients may occur at substantially higher levels. Therefore, this conservative condition was used to assess analytical tolerance and support the selectivity of the proposed platform.

Stability and reproducibility of the LIG sensor

The reproducibility of the LIG for CPX determination was assessed through inter-electrode assays using eight fabricated electrodes (n = 8). All electrodes were subjected to the same electrochemical activation protocol adopted in this study. The analytical response was subsequently recorded by differential pulse voltammetry in the presence of 40.0 µmol L^{-1} CPX, and the anodic peak current (Ip_a) was measured. The variability among sensing units was expressed as standard deviation (SD) and relative standard deviation (RSD, %) calculated from the Ip_a values obtained for each electrode.

The intra-electrode stability (multi-day performance) was evaluated using a single activated electrode, whose response was monitored over a period of 15 days under identical experimental conditions (DPV measurements in a solution containing 40.0 µmol L^{-1} CPX). On each evaluation day, the anodic peak current was determined, and the results were expressed in terms of SD and RSD (%).

Application to real samples

The applicability of the developed LIG sensor was evaluated using river water and pharmaceutical samples. River water was collected in Tiradentes, MG, Brazil (21.05450° S, 44.22231° W) following a previously described protocol.[25] The samples were filtered to remove suspended solids and were subsequently used to prepare CPX solutions. Spike recovery experiments were performed by fortifying the water samples with CPX at three concentration levels: 40.0, 60.0, and 70.0 µmol L^{-1}.

A commercial pharmaceutical formulation containing 500 mg of ciprofloxacin per tablet was analyzed. Tablets of known mass were dissolved in water to obtain suitable concentrations for electrochemical analyses. Recovery studies were conducted using the standard addition method, in which known amounts of CPX were added at three concentration levels: 8.0, 40.0, and 60.0 µmol L^{-1}. In both matrices, a calibration curve was applied to calculate recovery values, which validated the accuracy of the proposed method.

RESULTS AND DISCUSSION

EIS characterization of the LIG electrode

EIS was performed on the unmodified LIG electrode, and the resulting Nyquist diagram is shown in Figure 2. The equivalent circuit that best fitted the experimental data was the Voigt model with two-time constants. Across 20 independent LIG replicas, the mean standard deviation (±SD) of the fitted parameters for each circuit element is presented in Table I.

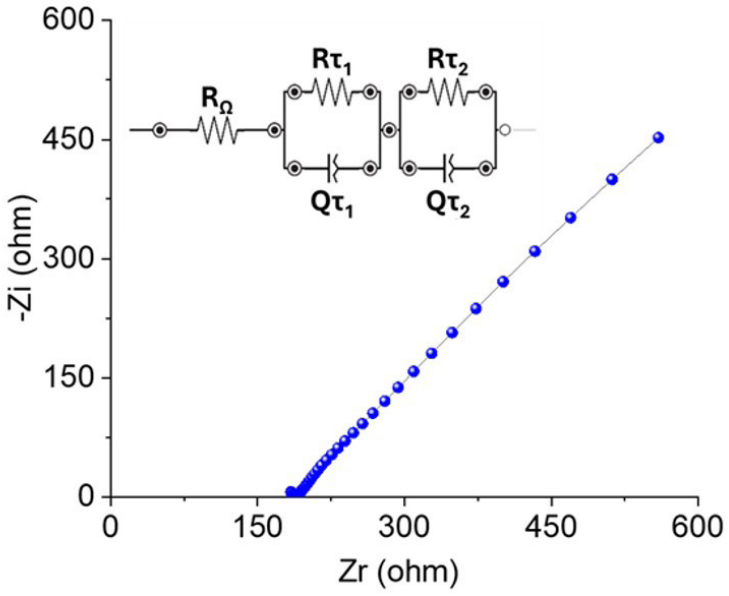

Figure 2. Nyquist plot of the unmodified LIG electrode obtained by EIS in a 5.0 mmol L^{-1} ferri/ferrocyanide redox probe ($[Fe(CN)_6]^{3-/4-}$, 1:1) solution prepared in 0.10 mol L^{-1} KCl solution.

Table I. EIS-derived parameters for the unmodified LIG (Voigt, Two Time Constants)

	LIG	
	Mean	**SD**
R_Ω (Ω)	159.0	5.0
$R\tau_1$ (Ω)	20.4	1.1
$Q\tau_1$ (μF)	210	21
***n*τ_1**	0.39	0.02
$R\tau_2$ (Ω)	5595	524
$Q\tau_2$ (mF)	3.3	0.41
***n*τ_2**	0.60	0.01

Values are mean ± SD, *n* = 20.
Electrolyte: 5 mmol L^{-1} $[Fe(CN)_6]^{3-/4-}$ in 0.1 mol L^{-1} KCl.

The high-frequency time constant (τ_1), assigned to interfacial charge transfer and double-layer formation at the working electrode, is smaller than the low-frequency time constant (τ_2), which reflects diffusion-affected processes within the internal/porous domains of LIG. This behavior is consistent with the irregular and heterogeneous LIG morphology, which yields multiple relaxation pathways and distributed time constants.[26] Moreover, the constant-phase element response (Qτ) indicates a dominant capacitive contribution relative to the resistive branch (Rτ). As the faradaic pathway becomes less significant than the capacitive pathway in each parallel element, the corresponding semicircle is poorly resolved. In our spectra, both semicircles are weakly defined, supporting that Qτ largely outweighs Rτ.[26]

The EIS response of two-time constants with depressed semicircles and low high-frequency resistance indicates fast interfacial charge transfer on a porous, high-area LIG surface with a pronounced capacitive coupling. After confirming a favorable LIG response, we optimized the experimental parameters for CPX to ensure reproducibility across independent replicates.

Optimization of experimental parameters for the LIG electrode

Electrochemical activation of LIG

Figure 3A compares the cyclic voltammograms recorded at the untreated electrode and after the electrochemical activation step. In both cases, a single irreversible anodic peak was observed near +0.70 V, consistent with CPX oxidation, which has been commonly associated with transformations at the piperazine moiety.

Mechanistic studies indicate that this anodic process predominantly involves oxidation of the piperazine tertiary amine, with initial electron abstraction to form a radical cation intermediate, followed by deprotonation and subsequent chemical transformation. This behavior is consistent with a proton-coupled electron-transfer (PCET) pathway proposed for CPX oxidation on graphitic/carbon surfaces.[27,28]

Following activation, the anodic peak current increased by 68%, indicating enhanced sensitivity. This trend agrees with reports showing that CPX oxidation is strongly influenced by interfacial adsorption and electrostatic interactions on carbon electrodes, and that a higher density of edge/defect sites and oxygenated functionalities increases adsorption sites and improves interfacial electron-transfer kinetics, thereby amplifying CPX signals.[29]

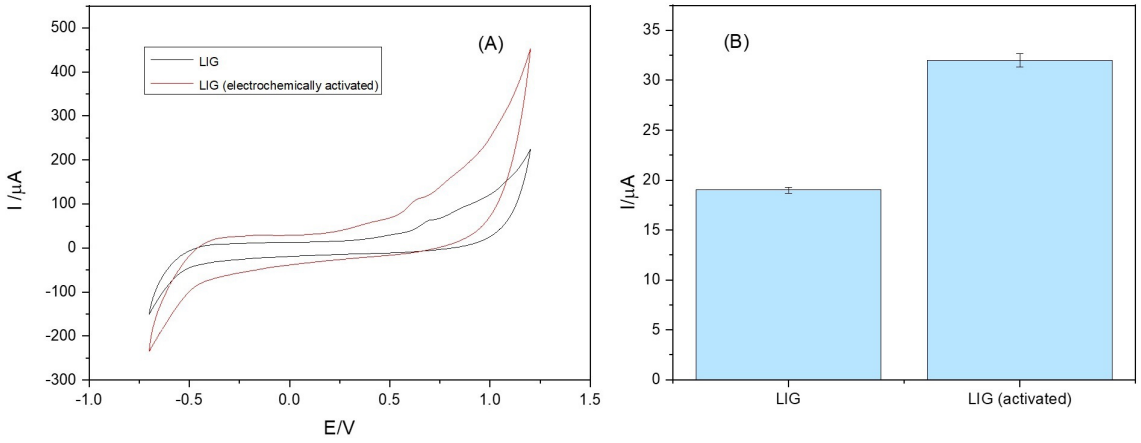

Figure 3. (A) Cyclic voltammograms recorded before and after electrochemical activation of the LIG electrode. (B) Dependence of the anodic peak current on the electrode activation process. Experiments were performed in 0.10 mol L^{-1} phosphate buffer (pH 7.0) containing 333 µmol L^{-1} CPX.

pH Effect

The influence of pH (4.0–10.0) on CPX oxidation at the activated LIG electrode was systematically investigated (Figure 4). The highest anodic peak current (Ip_a) was obtained at pH 7.0, whereas Ipa decreased markedly at pH 9.0–10.0. This trend is consistent with the acid–base speciation of CPX and its impact on interfacial preconcentration. At alkaline pH, the predominance of anionic CPX, together with changes in surface charge associated with oxygenated groups, disfavors adsorption and reduces interfacial electron-transfer efficiency, leading to a lower faradaic response.[30]

A linear shift of the anodic peak potential (Ep_a) toward less positive values with increasing pH was observed (Figure 4B), with a slope of 0.069 V pH^{-1}. This value is close to the theoretical Nernstian slope of 0.059 V pH^{-1} at 25 °C, indicating proton involvement and suggesting an approximately equal number of protons and electrons in the rate-determining step.[27,31] Mechanistic studies on fluoroquinolones further

propose that oxidation at the piperazine moiety proceeds via electron abstraction at the tertiary amine followed by deprotonation, consistent with an overall $2e^-/2H^+$ process.[28] Therefore, a pH of 7.0 was selected for the subsequent measurements.

Supporting electrolyte: Buffer composition and ionic strength

To assess the effect of the supporting electrolyte on the electrooxidation of CPX at the LIG electrode, we compared three buffer systems: phosphate, Britton–Robinson (BR), and Trizma, each at 0.10 mol L^{-1} and pH 7.0, thereby keeping the ionic strength constant. As shown in Figure 4C, phosphate and BR produced the highest responses, whereas Trizma produced a lower response. Considering both the electrochemical performance and practical aspects (availability of reagents, straightforward preparation, effective buffering near neutrality), a phosphate buffer (0.10 mol L^{-1}, pH 7.0) was selected for the subsequent experiments.

To elucidate the effect of ionic strength on CPX electrooxidation at the LIG electrode, the concentration of the supporting electrolyte (phosphate buffer, pH 7.0) was varied in the range of 0.05–0.30 mol L^{-1}, with all other parameters held constant. As shown in Figure 4D, the anodic peak current increased from 0.05 to 0.10 mol L^{-1}, consistent with a lower solution resistance (reduced iR drop) and adequate suppression of the migration. At concentrations >0.10 mol L^{-1}, the current decreased, likely due to specific ion–analyte and ion–surface interactions that hindered the charge transfer. Accordingly, 0.10 mol L^{-1} offered the best balance between conductivity and mass transport and was used for subsequent measurements.

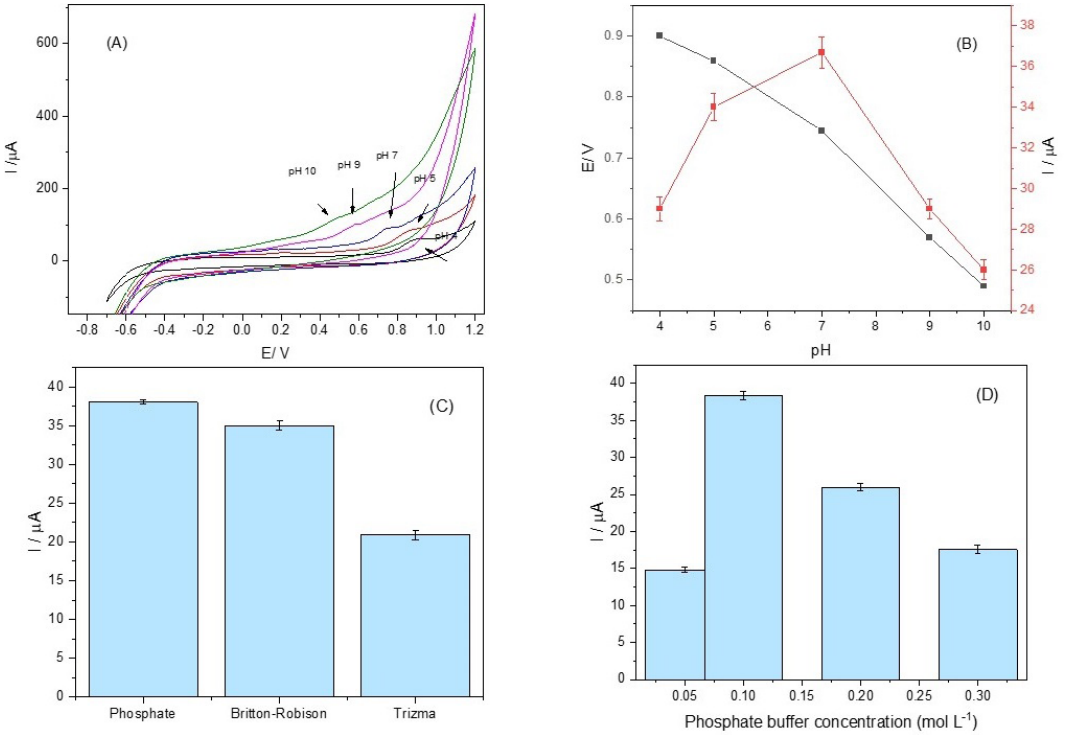

Figure 4. Optimization of the experimental parameters of the LIG electrode. (A) Cyclic voltammograms recorded at different pH values in 0.10 mol L^{-1} Britton–Robinson buffer. (B) Effect of pH on the anodic peak current of CPX obtained by cyclic voltammetry. (C) Effect of buffer identity on the anodic peak current of CPX (0.10 mol L^{-1} buffer, pH 7.0). (D) Effect of phosphate buffer ionic strength (pH 7.0) on the anodic peak current of CPX. In all experiments, the CPX concentration was 333 µmol L^{-1}.

Analytical calibration for CPX at the LIG electrode

Under the optimized DPV conditions, the anodic peak current increased linearly with ciprofloxacin concentration from 8.3–166.7 μmol L^{-1}, as shown (Figure 5).

$$Ip_a\ (\mu A) = 0.180\ [CPX]\ (\mu mol\ L^{-1}) + 0.207\ \mu A\ (R^2=0.99886)$$

Therefore, the sensitivity (slope) is 0.180 μA·L·μmol^{-1}. Using the blank standard deviation and the calibration slope, detection and quantification limits were estimated as LOD = $3SD_{blank}/b$ and LOQ = $10SD_{blank}/b$ where SD_{blank} is the standard deviation of 10 replicate blank measurements, and b is the slope (sensitivity) of the analytical calibration curve obtained by linear regression,[32] giving LOD = 2.5 μmol L^{-1} and LOQ = 8.3 μmol L^{-1}.

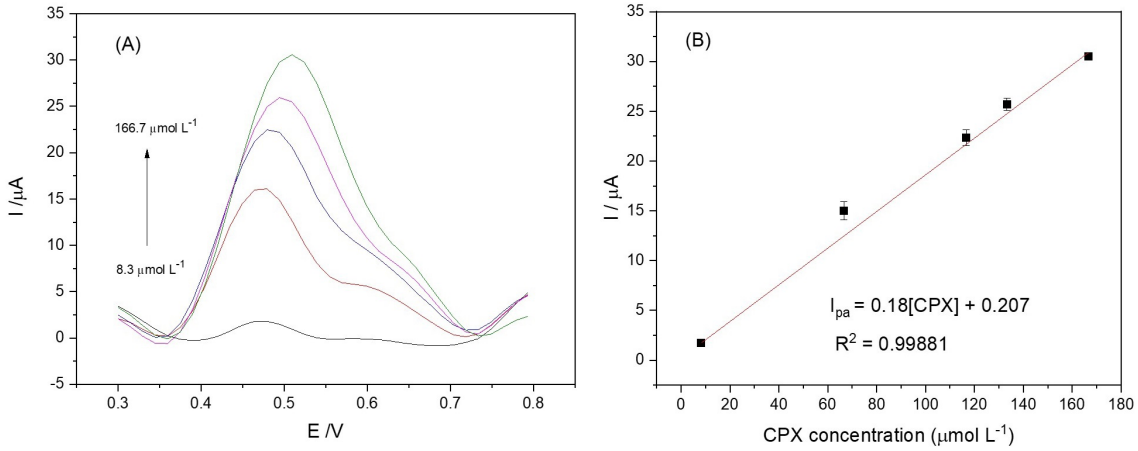

Figure 5. (A) Differential pulse voltammograms obtained upon successive additions of CPX. (B) Calibration curve constructed from the voltammograms shown in Figure 5A. Supporting electrolyte: 0.10 mol L^{-1} phosphate buffer (pH 7.0).

The laser-induced graphene (LIG) electrode exhibited excellent analytical performance for CPX detection, combining a low LOD and LOQ with high sensitivity, supporting its use in routine CPX monitoring. Accordingly, the method was applied to real samples to demonstrate its practical applicability in real-world scenarios.

Interference study

In the interference assessment, tetracycline (6.6%) and amoxicillin (5.4%) had the most pronounced effects on the results. All other tested species caused signal variations of less than 5% (Figure 6), confirming the high selectivity of the LIG sensor for CPX under these conditions.

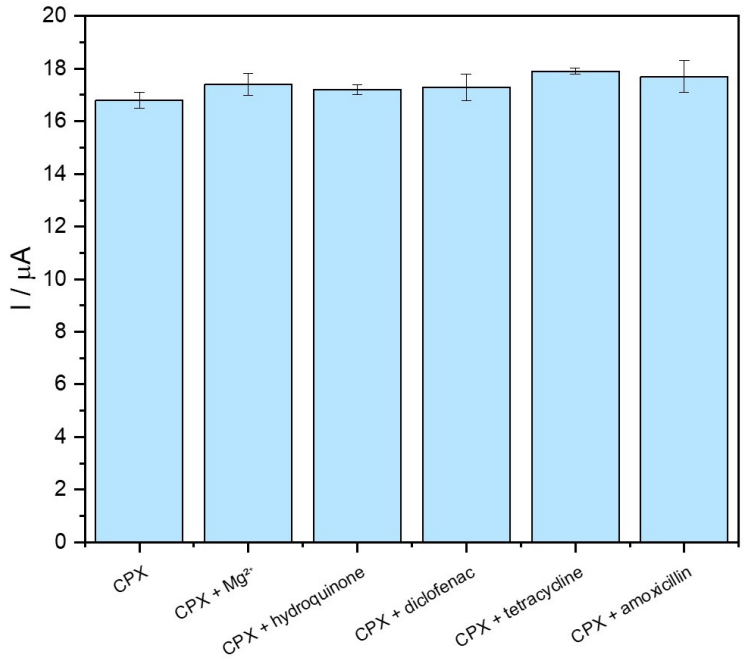

Figure 6. Interference study: anodic peak current of CPX in the presence of individual potential interferents. Error bars represent relative standard deviation (RSD, *n* = 3).

Stability and reproducibility of the LIG sensor

The reproducibility of the method for CPX determination was demonstrated by the analysis of eight independent sensors, fabricated under identical conditions, which showed an RSD of 4.1% (Figure 7A).

The long-term stability of the LIG electrode was evaluated by monitoring its response over 15 days (Figure 7B). Daily measurements of the anodic peak current yielded an RSD of 2.74%, with a total current decrease of only 7.5% by the end of the evaluation period.

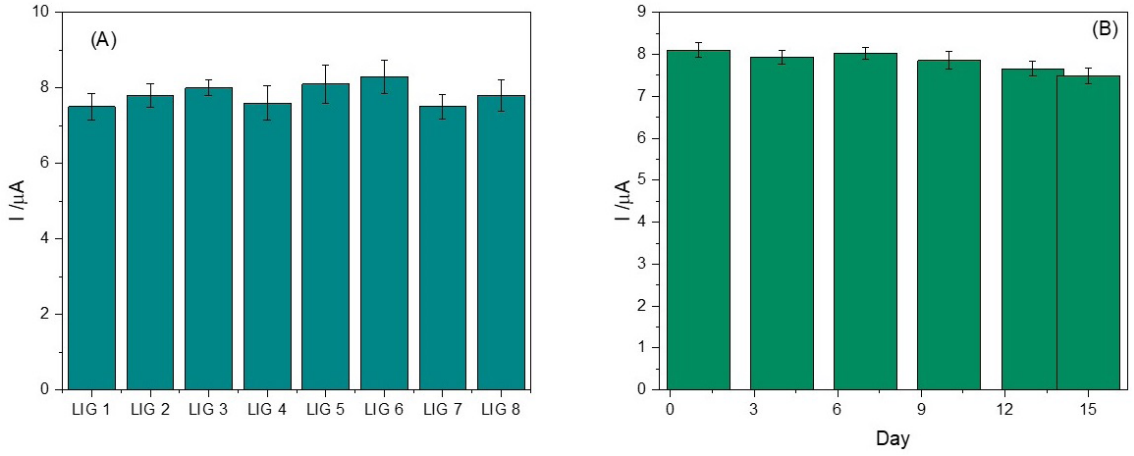

Figure 7. (A) Inter-electrode reproducibility evaluated for eight independently fabricated and activated LIG sensors (*n* = 3); (B) Multi-day stability of an activated LIG sensor monitored over 15 days (*n* = 3).

Application of the LIG to real samples

The LIG-based sensor afforded a LOD of 2.5 μmol L^{-1} for CPX, which is commensurate with concentrations documented in impacted waters (≈7.54–19.62 μmol L^{-1} in surface waters) and remains well below levels reported for pharmaceutical effluents (up to ≈93.6 μmol L^{-1}).[33] Consequently, the method is suitable for the direct detection and quantification of CPX in natural waters and for routine effluent monitoring, without the need for extensive preconcentration.

The proposed LIG-based electroanalytical method was successfully applied to determine CPX in river water and pharmaceutical formulations using a standard addition–recovery approach (Figure 8). In Figure 8A, the contribution near +0.7 V at the lowest spiking level is attributed to the low signal-to-noise ratio, with baseline currents from the LIG surface and matrix, characteristics associated with oxygenated functionalities and pseudocapacitive contributions.[16,23,25] As the CPX concentration increases, the faradaic signal predominates. The anodic peak shifts from +0.59 V to +0.66–0.69 V at higher concentrations, which is attributed to peak shape evolution and overlap with matrix contributions, similar phenomena observed in fluoroquinolone sensors.[27,30,31] Recovery results, shown in Tables II and III, confirm the reliability of the proposed approach, with excellent recovery values ranging from 92.93% to 110%, and low relative standard deviations (RSD < 3.80%), demonstrating the accuracy, precision, and robustness of the method for these samples.

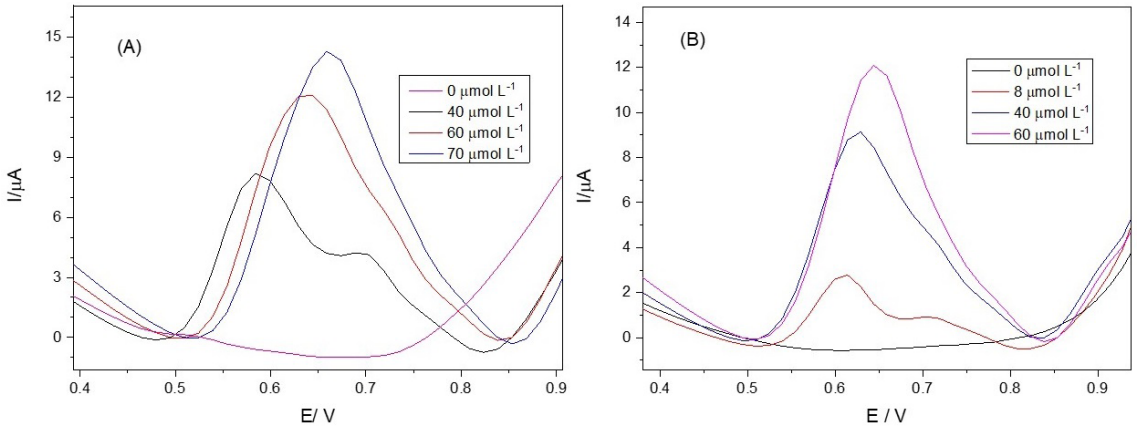

Figure 8. Differential pulse voltammograms obtained for the determination of CPX in: (A) pharmaceutical formulation sample and (B) river water sample. Measurements were performed in 0.10 mol L^{-1} phosphate buffer (pH 7.0).

Table II. Recovery results for CPX in pharmaceutical samples

Added (μmol L^{-1})	Found (μmol L^{-1})	RSD*	Recovery (%)
40.0	37.17	1.10	92.93
60.0	66.0	3.12	110
70.0	71.4	1.82	102.00

* n = 3

Table III. Recovery results for CPX in river water samples

Added (μmol L^{-1})	Found (μmol L^{-1})	RSD*	Recovery (%)
0	Not detected	–	–
8.0	7.5	3.80	93.75
40.0	43.10	3.49	107.75
60.0	59.22	1.20	98.70

* $n = 3$

Table IV compares the analytical performance of the proposed LIG sensor with representative electrochemical electrodes reported for CPX determination in different matrices. Sensors relying on nanocomposite-modified interfaces (e.g., Fe_3O_4/NPC/GCE or $La_2O_2CO_3$/GCE) commonly achieve lower LODs but typically require additional materials and wet-chemistry steps for electrode modification. In this work, the LIG sensor reached an LOD of 2.5 μmol L^{-1} and a practical linear range of 8.3–166.7 μmol L^{-1}, which enabled reliable CPX quantification in river water and pharmaceutical formulations within a straightforward analytical workflow.

Importantly, the novelty of the present study is not centered on achieving the lowest LOD, but on demonstrating a modifier-free LIG platform fabricated directly by laser scribing (solvent-free, no wet-chemistry functionalization) that combines operational simplicity, low cost, and surface robustness (chemical/mechanical stability) with fit-for-purpose analytical performance for routine determinations.

Table IV. Analytical performance of LIG compared with other electrochemical sensors for CPX determination

Sensor / Technique	Sample	Linear range (μmol L^{-1})	LOD (μmol L^{-1})	Ref.
ZMO/GCE/SWV[a]	Food samples	0.1 – 10	0.019	34
Fe_3O_4/NPC/GCE/SWV[b]	Milk and honey	1.0 –10	0.002	35
TiO_2/PVA-GCE/DPV[c]	Rainwater	10 –120	0.04	36
$La_2O_2CO_3$/GCE/DPV[d]	Milk, honey, egg, marine water, river water, organic fertilizer, soil, and human urine samples	5.98 – 57.87	1.90	37
Laser-induced graphene sensor (LIG)/DPV	River water, pharmaceutical formulation	8.3 – 166.7	2.5	This work

a- ZMO-/GCE – glassy carbon electrode modified with bimetallic zirconium molybdate; SWV - square wave voltammetry;
b- Fe_3O_4/NPC/GCE – glassy carbon electrode modified with ZIF-8 metal-organic framework (MOF)-derived N-containing porous carbon-supported Fe_3O_4 nanoparticles;
c- TiO_2/PVA-GCE – glassy carbon electrode modified with TiO_2/polyvinyl alcohol nanocomposite;
d- $La_2O_2CO_3$/GCE – glassy carbon electrode modified with lanthanum oxycarbonate nanoparticles.

CONCLUSIONS

Electrochemical impedance spectroscopy confirmed rapid interfacial charge transfer on the laser-induced graphene surface, and electrochemical activation further enhanced the CPX oxidation sensitivity of the sensor. The analyte response was pH-dependent, peaking at pH 7.0, and the anodic peak potential shifted linearly with pH (0.069 V pH^{-1}), indicating proton-coupled electron transfer.

The method enabled accurate CPX determination in river water and pharmaceutical formulation, with high recovery and low RSD. Combined with direct, solvent-free fabrication and the chemical/mechanical

robustness of LIG, these results position the platform as a cost-effective and sustainable alternative for environmental and quality control monitoring of CPX, with an estimated cost of approximately USD 0.015 per unit.

Acknowledgements

The authors acknowledge the support of the Fundação de Amparo à Pesquisa do Estado de Minas Gerais (FAPEMIG), Conselho Nacional de Desenvolvimento Científico e Tecnológico (CNPq), and Coordenação de Aperfeiçoamento de Pessoal de Nível Superior (CAPES) – Brazil. The authors also acknowledge the Instituto Nacional de Tecnologias Alternativas para Detecção, Avaliação Toxicológica e Remoção de Contaminantes Emergentes e Radioativos (INCT-DATREM) for research support.

Conflicts of interest

The authors declare no conflict of interest.

Use of Artificial Intelligence (AI) tools

The authors declare that they used ChatGPT and Grammarly for language editing. The authors take full responsibility for the accuracy, integrity, and originality of the article and confirm that no AI tools were used to generate novel scientific ideas, independently analyze data, or replace the critical role of the authors.

REFERENCES

(1) Pan, Q.; Peng, Y.; Yang, A.; Yang, D. Development of a molecularly imprinted photoelectrochemical sensor for enhanced detection of ciprofloxacin in milk. *Int. J. Electrochem. Sci.* **2023**, *18* (12), 100393. https://doi.org/10.1016/j.ijoes.2023.100393

(2) Vu, T. T.; Nguyen, M. C.; Dao, T. C.; Luu, T. H.; Luong, T.-Q. N. Trace detection of ciprofloxacin antibiotic using surface-enhanced Raman scattering coupled with silver nanostars. *Optik* **2022**, *260*, 169043. https://doi.org/10.1016/j.ijleo.2022.169043

(3) Mazzoni, L.; Abollino, O.; Fabbri, D.; Marafante, M.; Locatelli, M.; Perrucci, M.; Giacomino, A.; Inaudi, P. Portable electrochemical sensor for trace analysis of ciprofloxacin in water and pharmaceutical samples. *Microchem. J.* **2025**, *218*, 115295. https://doi.org/10.1016/j.microc.2025.115295

(4) Yuan, C.; He, Z.; Chen, Q.; Wang, X.; Zhai, C.; Zhu, M. Selective and efficacious photoelectrochemical detection of ciprofloxacin based on the self-assembly of 2D/2D g-C_3N_4/Ti_3C_2 composites. *Appl. Surf. Sci.* **2021**, *539*, 148241. https://doi.org/10.1016/j.apsusc.2020.148241

(5) Yang, S.; Li, K.; Sun, N.; Liu, J.; Luo, Q.; Zhang, Y.; Wang, L.; Wu, S.; Zhu, M. A lanthanide metal-organic framework for highly selective and sensitive fluorescence detection of ciprofloxacin. *Inorg. Chem. Commun.* **2023**, *158*, 111641. https://doi.org/10.1016/j.inoche.2023.111641

(6) Munir, F.; Waseem, M. T.; Khan, Z. A.; Majeed, S.; Farooq, U.; Shahzad, S. A. Synthesis of AIEE active triazine based new fluorescent and colorimetric probes: A reversible mechanochromism and sequential detection of picric acid and ciprofloxacin. *J. Photochem. Photobiol. A Chem.* **2022**, *429*, 113921. https://doi.org/10.1016/j.jphotochem.2022.113921

(7) Sharma, G.; Pahade, P.; Durgbanshi, A.; Carda-Broch, S.; Peris-Vicente, J.; Bose, D. Application of micellar liquid chromatographic method for rapid screening of ceftriaxone, metronidazole, amoxicillin, amikacin and ciprofloxacin in hospital wastewater from Sagar District, India. *Total Environ. Res. Themes* **2022**, *1–2*, 100003. https://doi.org/10.1016/j.totert.2022.100003

(8) Elgendy, K.; Zaky, M.; Eldin, T. A.; Fadel, S. Rapid HPLC determination of ciprofloxacin, ofloxacin, and marbofloxacin alone or in a mixture. *Results Chem.* **2023**, *5*, 100749. https://doi.org/10.1016/j.rechem.2022.100749

(9) Nadar, A.; Jain, V.; D'Sa, M. Stability-indicating RP-HPLC method development and validation for simultaneous quantification of ciprofloxacin, curcumin, and piperine in a novel topical dosage form. *Microchem. J.* **2025**, *216*, 114554. https://doi.org/10.1016/j.microc.2025.114554

(10) Xiong, Y.; Zhang, D.; Ye, C.; Wang, Y.; Deng, X.; Deng, D.; Xiong, C.; Zhang, J.; Gu, Q.; Huang, G. Ultrasensitive detection of ciprofloxacin hydrochloride in milk by molecularly imprinted electrochemical sensor based on S-CoFe-MOFs/AuNPs. *J. Food Compos. Anal.* **2023**, *122*, 105439. https://doi.org/10.1016/j.jfca.2023.105439
(11) Adane, W. D.; Chandravanshi, B. S.; Tessema, M. A simple, ultrasensitive and cost-effective electrochemical sensor for the determination of ciprofloxacin in various types of samples. *Sens. Bio-Sens. Res.* **2023**, *39*, 100547. https://doi.org/10.1016/j.sbsr.2022.100547
(12) Wang, Q.; He, B.; Liu, Y.; Wang, Y.; Jiang, L.; Jin, H.; Wei, M.; Ren, W.; Suo, Z.; Xu, Y. An electrochemical aptasensor based on AuPt@PEI-g-C_3N_4 combined with a rolling circle amplification strategy for ultrasensitive detection of ciprofloxacin. *Microchem. J.* **2024**, *197*, 109871. https://doi.org/10.1016/j.microc.2023.109871
(13) Zhang, S.; Yu, S.; Wang, X.; Zhang, Y.; Yue, Z.; Li, C.; Ma, Y. An electrochemical sensor based on MnO_2/ZnO composites for the detection of ciprofloxacin in honey. *Microchem. J.* **2023**, *194*, 109355. https://doi.org/10.1016/j.microc.2023.109355
(14) Souza, C. C.; Alves, G. F.; Lisboa, T. P.; Matos, M. A. C.; Matos, R. C. Low-cost paper-based electrochemical sensor for the detection of ciprofloxacin in honey and milk samples. *J. Food Compos. Anal.* **2022**, *112*, 104700. https://doi.org/10.1016/j.jfca.2022.104700
(15) Shepa, J.; Király, N.; Demeterová, J.; Shepa, I.; Hviščová, P.; Volavka, D.; Kožár, M.; Šišoláková, I.; Oriňaková, R.; Zeleňák, V.; Almáši, M. Determination of ciprofloxacin using metal–organic frameworks-modified electrochemical sensors for environmental and clinical applications. *Microchem. J.* **2025**, *218*, 115638. https://doi.org/10.1016/j.microc.2025.115638
(16) Nasraoui, S.; Al-Hamry, A.; Madeira, T. I.; Ameur, S.; Zahn, D. R. T.; Ben Ali, M.; Kanoun, O. Structural characterization and electrochemical performance of laser-induced graphene: Insights into electron transfer kinetics and 4-aminophenol sensing. *Diamond Relat. Mater.* **2023**, *138*, 110207. https://doi.org/10.1016/j.diamond.2023.110207
(17) Shi, S.; Wu, C.; Zhu, Z.; Sun, S. Simple and Low-Cost Construction of a Sensitive Pb (II) Ions Electrochemical Sensor Using Cu Nanoparticles-Modified Laser-Induced Graphene. *Microchem. J.* **2025**, *218*, 115570. https://doi.org/10.1016/j.microc.2025.115570
(18) Luengrojanakul, P.; Klamchuen, A.; Leepheng, P.; Tunhoo, B.; Charoensuk, K.; Rimdusit, S. Shape memory laser-induced graphene electrode based on polybenzoxazine-co-epoxy coated fabric and its electrochemical sensor application. *Mater. Res. Bull.* **2025**, *192*, 113591. https://doi.org/10.1016/j.materresbull.2025.113591
(19) Marinho, J. Z.; Araújo, D. A. G.; Nascimento, L. L.; Patrocinio, A. O. T.; Trindade, M. A. G.; Matias, T. A.; Bonacin, J. A.; Paixão, T. R. L. C.; Muñoz, R. A. A. Laser-induced NiO-embedded graphene nanostructures: Single-step generation of nonenzymatic electrochemical sensors. *Mater. Sci. Eng., B* **2026**, *323*, Part A, 118701. https://doi.org/10.1016/j.mseb.2025.118701
(20) Setti, M.; Vaughan, E.; Murray, R.; Sygellou, L.; Quinn, A. J.; Riccò, M.; Pontiroli, D.; Iacopino, D. Sustainable electrochemical sensors from cork-derived laser-induced graphene: Non-enzymatic glucose detection in urine. *Sens. Actuators, B* **2025**, *430*, 137352. https://doi.org/10.1016/j.snb.2025.137352
(21) Yuan, X.; Wu, X.; Ling, Y.; Li, S.; Chen, J.; Zhang, Z. In situ bismuth ion exchange plating micro-electrochemical sensor based on laser-induced graphene for trace Cd^{2+} and Pb^{2+} detection. *J. Environ. Chem. Eng.* **2024**, *12*, 112161. https://doi.org/10.1016/j.jece.2024.112161
(22) Nong, J.; Zhang, N.; Wen, A.; Hu, C. Anti-biofouling laser-scribed graphene electrochemical sensor for reliable detection of uric acid in human saliva. *J. Electroanal. Chem.* **2024**, *952*, 117982. https://doi.org/10.1016/j.jelechem.2023.117982
(23) Liu, X.; Zhang, F.; Zhang, Q.; Wan, Z.; Chen, X. Laser-scribed graphene for sensors: preparation, modification, applications, and future prospects. *Light: Advanced Manufacturing* **2023**, *4*, 11. https://doi.org/10.37188/lam.2023.011

(24) Machado, Â.; Lima, T.; Coelho, R.; Figueiredo Dias, G.; Soares, P.; Martins, H.; Franco, D.; Pereira, A.; Franco, L. Optimizing laser-induced graphene oxide electrodes for electroanalytical applications using response surface methodology. *J. Solid State Electrochem.* **2025**, *29*, 855–872. https://doi.org/10.1007/s10008-024-06141-9
(25) Companhia Ambiental do Estado de São Paulo (CETESB); Agência Nacional de Águas (ANA). *Guia nacional de coleta e preservação de amostras: água, sedimento, comunidades aquáticas e efluentes líquidos.* São Paulo: CETESB; Brasília: ANA, 2011. https://www.clean.com.br/downloads/Guia_Nacional_de_Coleta_e_Preservacao_de_Amostras_.pdf (accessed 2024-01-28).
(26) Lasia, A. *Electrochemical Impedance Spectroscopy and its Applications*. 2nd ed. Springer, New York, 2014. https://doi.org/10.1007/978-1-4614-8933-7
(27) Crapnell, R. D.; Adarakatti, P. S.; Banks, C. E. Electroanalytical overview: the measurement of ciprofloxacin. *Sens. Diagn.* **2024**, *3* (1), 40–58. https://doi.org/10.1039/d3sd00129f
(28) Voigt, M.; Dluziak, J.-M.; Wellen, N.; Jaeger, M. Mechanistic study of the electrochemical oxidation of fluoroquinolones: Ciprofloxacin, danofloxacin, enoxacin, levofloxacin and lomefloxacin. *Chemosphere* **2024**, *355*, 141763. https://doi.org/10.1016/j.chemosphere.2024.141763
(29) Osaki, S.; Saito, M.; Nagai, H.; Tamiya, E. Surface Modification of Screen-Printed Carbon Electrode through Oxygen Plasma to Enhance Biosensor Sensitivity. *Biosensors* **2024**, *14*, 165. https://doi.org/10.3390/bios14040165
(30) Almada-Leyva, M. L.; Tecuapa-Flores, E. D.; Rojas, L. M. G.; Thangarasu, P. Ionic liquid and ZnO/carbon quantum dots derived from cat hair as an electrochemical sensor for ciprofloxacin in food samples: Experimental and cell-imaging studies. *Electroanalysis* **2024**, *36* (9), e202300398. https://doi.org/10.1002/elan.202300398
(31) Măgeruşan, L.; Pogăcean, F.; Cozar, B.-I.; Tripon, S.-C.; Pruneanu, S. Harnessing graphene-modified electrode sensitivity for enhanced ciprofloxacin detection. *Int. J. Mol. Sci.* **2024**, *25* (7), 3691. https://doi.org/10.3390/ijms25073691
(32) dos Santos, S. M. V.; Oliveira, P. R.; Oliveira, M. C.; Bergamini, M. F.; Marcolino-Jr, L. H. Eletrodos impressos construídos por serigrafia utilizando negro de fumo como material condutor. *Rev. Virtual Quim.* **2017**, *9* (2), 626–640. https://doi.org/10.21577/1984-6835.20170037
(33) Khan, P.; Saha, R.; Halder, G. Towards sorptive eradication of pharmaceutical micro-pollutant ciprofloxacin from aquatic environment: A comprehensive review. *Sci. Total Environ.* **2024**, *919*, 170723. https://doi.org/10.1016/j.scitotenv.2024.170723
(34) Afzal, M. H.; Pervaiz, W.; Elahi, N.; Huang, Z.; Li, G.; Liu, H. Development of a low-cost zirconium molybdate bimetallic center electrochemical sensor for simultaneous enrofloxacin and ciprofloxacin detection in food samples. *Microchem. J.* **2025**, *218*, 115165. https://doi.org/10.1016/j.microc.2025.115165
(35) Li, G.; Zhang, Y.; Zhu, R.; Liu, Z.; Jin, Y.; Ma, N.; He, X. An efficient electrochemical sensor based on ZIF-8 MOF-derived N-containing porous carbon supported Fe_3O_4 nanoparticles for sensitive detection of ciprofloxacin residues in foods. *Microchem. J.* **2025**, *218*, 115415. https://doi.org/10.1016/j.microc.2025.115415
(36) Zhao, J.; Huang, P.; Jin, W. Electrochemical sensor based on TiO_2/polyvinyl alcohol nanocomposite for detection of ciprofloxacin in rainwater. *Int. J. Electrochem. Sci.* **2021**, *16* (10), 211018. https://doi.org/10.20964/2021.10.01
(37) Chakravorty, A.; Das, S.; Luktuke, S.; Mini, A. A.; Raghavan, V. Electrochemical detection of enrofloxacin and ciprofloxacin based on mesoporous $La_2O_2CO_3$ nanostructures – an eco-friendly electrode material for sustainability. *Talanta Open* **2025**, *12*, 100546. https://doi.org/10.1016/j.talo.2025.100546